Published in final edited form as:
J Phys Chem Lett. 2013 April 4; 4(7): 1148–1155. doi:10.1021/jz4000142.

DNA-Templated Molecular Silver Fluorophores

Jeffrey T. Petty[§], **Sandra P. Story**[§], **Jung-Cheng Hsiang**[#], and **Robert M. Dickson**[#,*]
[§]Department of Chemistry, Furman University, Greenville, SC 29613

[#]School of Chemistry and Biochemistry and Petit Institute of Bioengineering and Bioscience, Georgia Institute of Technology, Atlanta, GA 30332-0400

Abstract

Conductive and plasmon-supporting noble metals exhibit an especially wide range of size-dependent properties, with discrete electronic levels, strong optical absorption, and efficient radiative relaxation dominating optical behavior at the ~10-atom cluster scale. In this Perspective, we describe the formation and stabilization of silver clusters using DNA templates and highlight the distinct spectroscopic and photophysical properties of the resulting hybrid fluorophores. Strong visible to near-IR emission from DNA-encapsulated silver clusters ranging in size from 5–11 atoms has been produced and characterized. Importantly, this strong Ag cluster fluorescence can be directly modulated and selectively recovered by optically controlling the dark state residence, even when faced with an overwhelming background. The strength and sequence sensitivity of the oligonucleotide-Ag interaction suggests strategies for fine tuning and stabilizing cluster-based emitters in a host of sensing and biolabeling applications that would benefit from brighter, more photostable, and quantifiable emitters in high background environments.

Keywords

Noble metals; clusters; modulation; fluorescence; biolabel; imaging; photophysics

Few-atom metal clusters exhibit distinctive, size-dependent behaviors along the transition from bulk to molecular scales. For example, as electron mean free path and Fermi screening length scales are approached, the excellent conductivity and optical reflectivity characterizing bulk metals morph into shape-dependent plasmon excitations, size-dependent redox potentials and chemical/biological reactivities, with discrete optical transitions emerging at even smaller sizes.[1–4] Resulting from their relative inertness and highly polarizable electronic transitions, molecular-scale noble metals have emerged as a promising class of fluorophores for materials and biological imaging. Characterized by excellent brightness and photostability, gold and silver clusters encapsulated by coordinating ligands feature strong optical transitions that vary not only with stoichiometry, charge, and geometry, but can also be strongly influenced by interactions with their encapsulating matrix.[5–8] As the molecular size scale is approached, few-atom metallic cluster sizes exhibit an insufficient density of states to close the “band gap” as occurs in bulk or nanoparticulate metals, leading to strong size-dependent optical and catalytic properties that in many cases are well-explained by the nuclear shell model for free electron energies and magic cluster sizes.[9–11] This approach has led to the extended atom description of metallic clusters and an effective expansion of the periodic table with size-dependent cluster behaviors when metal-metal interactions dominate cluster stability.[12, 13]

*dickson@chemistry.gatech.edu.

Although the protoplasmonic electronic structure of metal clusters is best observed in bare, unsolvated and isolated clusters,[9, 10, 14] ligands are essential to constrain growth, stabilize, and enable derivatization of solution-phase clusters. However, these ligand-cluster interactions often alter the jellium stabilities and scalings of optical properties identified in gas or low-temperature environments. While glutathione-capped gold clusters show intriguing jellium-like absorptions that scale with size, these materials exhibit only weak emission.[15] More weakly coordinating ligands promote stronger emission from gold clusters, but they remain incapable of directing the synthesis of pure, size-directed cluster emitters and enhancing their chemical and photochemical stability.[16] In parallel with developments characterizing size-dependent Au cluster emission, extremely bright and photostable Ag cluster emission was reported on room temperature silver/silver oxide films and by encapsulation in amine-based dendrimers.[17–19] Higher concentrations or introduction of buffer, however, immediately caused aggregation to form large Ag nanoparticles, thereby quenching the desired emission. Thus, any practical application needs to achieve a compromise between increased ligand-Ag cluster interaction and overall cluster brightness. These challenges and the need for improved biological labels suggested identifying peptide[20] and oligonucleotide[21] scaffolds in which electron-rich binding sites can be programmed through variations in the primary sequence of the encapsulating biopolymer. While initial success with peptide scaffolds was achieved,[20] the few percent quantum yields were difficult to optimize due to the great diversity of possible binding sequences. In contrast, the strong nucleobase-centered metal binding characteristic of DNA offered a simpler and more productive route to bright, tunable fluorophore creation.[21] Thus, oligonucleotide-encapsulated Ag clusters (Ag nanodots, Fig. 1) have become an excellent system to investigate size-dependent emission, understand unique photophysics, and simultaneously increase brightness and sensitivity in both in vitro fluorescence experiments and sensing applications, while holding promise for cost-effective, improved detection compatible with oligonucleotide nanotechnologies.

Silver cluster creation

Single-stranded DNA readily binds both silver ions and neutral silver clusters. The nucleobases exhibit affinities of $>10^5$ M^{-1} with Ag^+, and stable complexes form between Ag^+ and 10 – 30 nucleotide strands when both concentrations exceed 10 μM (Fig. 1A).[22, 23] Cluster growth is curtailed, however, by using Ag^+: nucleobase ratios significantly smaller than 1:2. Within several hours following Ag^+ reduction with borohydride, the development of silver clusters results in chiral spectroscopic signatures in the visible spectrum, silver-induced shifts in the mass spectra of monodisperse oligonucleotides, and hydrodynamic sizes that are dominated by the DNA scaffold.[21, 24, 25] These bound clusters are stabilized by complexation with the electron-rich, endocyclic nitrogens of the nucleobases, and coordination by cytosine is favored at neutral pH.[26–28] These conjugates can be made to be robust in aqueous buffers and in cell culture media, highlighting the strength of metal-nucleobase coordination in spite of competing oxidation and precipitation reactions.[20, 21, 29, 30] An appealing feature of DNA-conjugated silver cluster chromophores is that simple variation of the oligonucleotide template primary sequence produces distinct clusters with emission spanning the blue-green to near-infrared spectral region (Fig. 1B).[31] The DNA-silver interaction is also modulated by varying reaction conditions. For example, pH directly influences the degree of nucleobase ionization, while Na^+ concentration to alters phosphate neutralization.[21, 26, 31, 32] Beyond the bounds imposed by the DNA strand, reaction conditions can be manipulated to favor specific clusters, and mild oxidizing conditions are used to enrich blue and green emitting clusters as well as non-emissive violet absorbing species.[25, 27, 33] This selective reactivity likely partially arises from size-dependent variations in cluster oxidation potentials.[3]

Characterization

Although size-dependent electronic configurations of metal clusters likely play an important role in cluster stability, the strongly interacting and protective DNA scaffold must also direct cluster size and influence electronic properties. Electrospray ionization mass spectrometry (ESI-MS) clearly shows that free-electron gas-phase electronic stabilities are, by themselves, insufficient to explain often polydisperse DNA-encapsulated silver cluster populations and final optical properties.[34] In ESI-MS, liquids are charged and aerosolized, followed by solvent evaporation prior to mass spectral analysis. Thus, while optical properties of solution-stable species are measured, mass spectral abundances of species stable in the gas phase are measured. Even if starting from chemically pure cluster solutions, it is not clear that these solution and gas-phase stabilities of DNA-encapsulated metal clusters are sufficiently similar to infer sizes of solution-phase cluster emitters. More importantly, spectral purity in the emission spectrum does not guarantee chemical purity, as synthetic methods yield multiple absorption bands associated with distinct types of clusters.[35, 36] Further, as solvent evaporation often alters the distribution of weakly-coordinated species in solution, the combined rapid evaporation and potential for Coulomb explosion at high charge densities unique to electrospray ionization potentially convolves gas and solution phase stabilities in ESI-MS size determinations. Thus, in situ stoichiometry estimates of specific emissive species remain technically challenging. [34, 37]

Preferring a more chemical approach, we have successfully purified specific cluster emitters, followed by combined spectroscopic and elemental analyses to quantify DNA, silver, and cluster stoichiometries.[33, 35, 36] Specific conjugates are resolved and purified using reversed-phase and size-exclusion chromatographies because silver clusters perturb the polarity and shape of their DNA hosts.[33, 35, 36] Subsequent isolation and atomic emission measurements from silver and phosphorus provide the silver:oligonucleotide ratio composing a given emitter. With the purified samples, the relative proportions of cluster and DNA are measured using the absorption spectra, which exhibit clearly resolved DNA and silver cluster absorptions on an otherwise flat baseline (Fig. 2). By comparing these absorbances, the relative cluster:DNA concentrations are derived using the extinction coefficients obtained from combined fluorescence correlation (FCS) and absorption spectroscopies.[36] To date, both emissive and non-emissive species with 5–11 silver atoms:DNA have been characterized (Table 1). Unlike gold clusters with very weakly coordinating ligands,[13] neither a suggestive trend nor the appropriate sizes for free-electron scaling of electronic transition energies is observed, as illustrated by the orange emission from five-atom clusters. Thus, while Ag cluster size does appear to be the major determinant of optical properties, the DNA-Ag interaction also strongly influences cluster properties. This integral impact of DNA is further accentuated by the fact that even single nucleobase changes within the template $C_3AC_3AC_3XC_3Y$ can produce large shifts in photophysics, shifting absorption and emission, for example, by more than 100 nm (Table 1).[35] New opportunities to explore an even broader range of cluster-DNA conjugates will arise as separation methodologies are refined.[38] Comparative studies using both atomic emission and mass spectrometry would advance our understanding of cluster size, and preliminary studies are encouraging.[38] A starting point for such studies might be to consider particular clusters that are favored by particular DNA structures and by oxidizing conditions.[25, 27] Further, although elemental analyses cannot discriminate between single 5–11 atom clusters and multiple smaller clusters per DNA strand, the mirror-image absorption and emission spectra that shift throughout the visible spectrum and the very similar (~3ns) lifetimes for all emitters tend to support our interpretation of single Ag clusters that vary in size instead of a distributed set of tiny, but electronically coupled clusters along the DNA strand.

Photophysical Properties

Restricted to a small number of atoms, silver clusters embedded within DNA exhibit molecule-like photophysical behavior. First, molar absorptivities of $>10^5$ $M^{-1}cm^{-1}$ have been derived by directly enumerating in situ cluster concentrations using FCS.[24, 31, 35, 36, 39] Measured extinction coefficients are similar to or slightly exceed those for the single electron transitions in organic dyes.[31] Second, fluorescence quantum yields ranging from 10–70%, in conjunction with high photostability, demonstrate that clusters stabilized within DNA matrices dissipate much of their absorbed energy through radiative relaxation.[31, 32, 35] These properties improve net fluorescence brightnesses of silver clusters beyond those of the best available organic dyes in each spectral region.[40] Further, two photon fluorescence brightnesses approach those of much larger semiconductor nanocrystals.[24, 41] Largely resulting from nucleobase-induced stabilization, encapsulated cluster radiative relaxation contrasts sharply with Ag atom- or electron-ejection excited state decay characteristic of bare clusters.[3] Thus, the DNA scaffold is crucial to the excellent brightness and photostability of one- and two-photon-excited emission.

Photobrightening

While maximizing radiative decay is crucial to fluorophore brightness, understanding and controlling transitions to dark electronic states has enabled a host of new imaging schemes.[42–47] Stemming from its role in cluster stabilization, the DNA scaffold corrals the photoejection-related decay channels characteristic of gas phase clusters to offer a novel path employing sequential two-photon absorption for dramatic improvements in sensitivity via long-wavelength, laser-induced fluorescence enhancement (Fig. 3).[48–50] Although relatively short compared to most organics and quantum dots, the ~30 μs cluster dark state residence remains long compared with the ns fluorescence lifetime, resulting in buildup of sizeable (>50%) steady-state dark state populations under moderate excitation intensity. All investigated clusters possess strikingly similar, long-wavelength dark state absorptions that suggest transient formation of anionic cytosine upon cluster photoexcitation. Optical excitation of this broad, long-wavelength transient absorption rapidly transfers dark state population back to the bright manifold, thereby enhancing the steady state emission by a factor of $1 + \tau_{off}/\tau_{on}$, where τ_{off} is the dark state lifetime and τ_{on} is the time spent in the emissive manifold prior to reaching the dark state.[48–50] Thus, overall brightness is increased several-fold through intervening optically to curtail residence in the dark state. Because low-energy co-illumination generates no fluorescence background, spectral filtering isolates the laser-magnified emission, and the rate of dark state decay is controlled via secondary laser intensity.

Fluorescence modulation and signal recovery

Photobrightening of Ag cluster emission through long-wavelength secondary illumination presents a unique opportunity in fluorescence imaging and detection. Secondary laser co-illumination shifts the steady-state populations within the dark and bright state manifolds, but this shift occurs over a characteristic timescale, $\tau_c = (k_{on}+k_{off})^{-1}$, with $k_{on} = \tau_{on}^{-1}$ and $k_{off} = \tau_{off}^{-1}$ being the rate of transition out of the fluorescence-generating manifold of states (product of excitation rate and dark state quantum yield) and the rate constant for dark state decay, respectively. This characteristic time to re-establish the new steady-state populations simultaneously provides a measure of the dark state lifetime (k_{off}^{-1}), and the ability to modulate dark state populations over periods longer than τ_c. Temporal modulation of the secondary laser intensity thus directly encodes the secondary laser modulation waveform on the collected fluorescence intensity by dynamically altering steady-state ground state population. Fourier transformation of collected bulk or single molecule fluorescence allows

efficient extraction of cluster emission from other background contributions (Fig. 3B–C).[49] The common transient absorption of all DNA-Ag clusters[48] makes all known clusters modulatable at similar (~800nm) wavelengths. The dark state lifetimes (k_{off}^{-1}) and overall extinction coefficients determine the characteristic modulation frequencies (τ_c^{-1}) and maximum modulation depths ($1+ \tau_{off}/\tau_{on}$).[35, 50] Thus, all cluster emitters can be modulated and selectively detected in the presence of overwhelming background. Unlike the inverse concentration dependence of fluorescence correlation spectroscopy, the modulation amplitude in the Fourier spectrum is linear with the number of cluster emitters. This enables accurate concentration determinations from mM to the single molecule level, even when background is an order of magnitude higher than analyte signal (Fig. 3). Modulation of these species has been utilized in fixed cell imaging (Fig. 4),[49] and upon transferring these concepts to more standard fluorescent proteins, modulatable and unmodulatable protein emitters have been directly distinguished in live cells.[45]

Molecular Sensors

Many analytes that associate with DNA will also appear to perturb the original DNA-silver interaction, thereby shifting the distribution of chromophores associated with the host DNA strand. Having many important applications on its own, detection of DNA strands also provides a robust model to understand this analyte response because base pairing and stacking interactions allow both the structure and affinity of the resulting complex to be accurately predicted. Further, subtle variations in affinity can be achieved through mismatches,[51, 52] and relatively minor changes in the secondary and tertiary structure of the host strand can dramatically alter the cluster-binding environment. Thus, through proper design of the DNA template, large intensity and spectral changes can be linked with DNA recognition, as demonstrated by distant mismatch-induced allosteric changes, proximal positioning of DNA strands, and hybridization-driven changes in DNA shape (Fig. 5).[33, 51–56] These cases provide a foundation to understand how a broader class of analytes can produce DNA structural changes that elicit spectroscopically resolvable changes in the cluster binding site. Especially when used to generate either modulatable or near infrared-emitting species upon target recognition, these encapsulated clusters offer exciting opportunities in sensing by utilizing their high brightness and drastic background removal upon modulation.

Future directions

DNA-encapsulated silver clusters (a.k.a. Ag nanodots) are promising new fluorophores that improve on organic dye brightness and photostability while maintaining moderate size and biocompatibility. Tunable both through cluster size and scaffold interactions, the photophysics support optical modulation of cluster fluorescence for selective recovery, even when buried within otherwise overwhelming background. Thus, while challenges in elucidating design criteria, targeting schemes, and overall intracellular and in vivo stabilities remain, applications as in vitro fluorescent labels, especially for sensing and DNA nanotechnology diagnostics appear particularly promising. The ability to discriminate cluster signals in high background environments suggests fewer processing steps may be necessary for visualization of desired response. The propensity of silver to oxidize and the poor solubility of silver salts remains a limiting issue in complex media, however. While scaffolds have been tuned to enable direct synthesis in complex cell culture media, and ~10 minute intracellular survival,[39] more strongly chelating peptide scaffolds[20] may offer promising paths to stable, highly emissive, and genetically encodable Ag cluster labels (Fig. 6). Initial successes demonstrate the promise of such materials, but vast peptide diversity provides a significantly larger optimization space than available to DNA. Thus, identification and optimization of new silver cluster-binding scaffolds promise the ability to

further tailor nanoconjugate properties to nearly any envisionable biological or materials application.

Structural and energetic studies will also provide a foundation for further development of these metal-based chromophores. In this Perspective, we have focused on the clusters, whose stability at room temperature in aqueous buffers relies on nucleobase coordination. From the complementary perspective, complexation with the metallic cluster alters the shape and structure of the DNA host, and these changes depend not only on the primary sequence of the DNA strand and the type of cluster, but also on the reaction conditions and the buffer environment. To better produce specific clusters and optimize their photophysical properties, spectroscopic techniques such as nuclear magnetic resonance could be used. Such efforts will require larger amounts of purified conjugates than is currently needed for absorption or fluorescence spectroscopies. These efforts will be advanced as synthetic techniques are improved to yield higher purity samples under a wider range of conditions. The impact of these ligands is already evident in studies that show cluster-induced conformational changes, and these alternative polymorphic forms could be utilized for the recognition of specific analytes. The improved thermal and chemical stabilities of ligand-Ag cluster conjugates must be understood and achieved under a much wider range of conditions, however, for more applications of these species to materialize. Once achieved, improved understanding, stability, control, and prediction of strongly absorbing, size/ligand-tunable energy levels of noble metal clusters is likely to impact fields as diverse as cluster physics, catalysis, spectroscopy, imaging, sensing, and fluorophore development far into the future.

Acknowledgments

The authors gratefully acknowledge support from NIH R01 GM086195 (RMD). JP is grateful for the following support: National Science Foundation (CBET-0853692, CHE-0922834, CHE-0718588, and the Regional NSF-REU Site in Chemistry at Furman University), the National Institutes of Health (R15GM071370), the Henry Dreyfus Teacher-Scholar Awards Program, the Howard Hughes Medical Institute (USE Award to Furman University), and support from the Henry Keith and Ellen Hard Townes Professorship.

References

1. Lohse SE, Murphy CJ. Applications of Colloidal Inorganic Nanoparticles: From Medicine to energy. J Amer Chem Soc. 2012; 134:15607–15620. [PubMed: 22934680]
2. Jain PK, Huang X, El-Sayed IH, El-Sayed MA. Noble Metals on the Nanoscale: Optical and Photothermal Properties and Some Applications in Imaging, Sensing, Biology, and Medicine. Acc Chem Res. 2008; 41:1578–1586. [PubMed: 18447366]
3. Henglein A, Mulvaney P, Linnert T. Chemistry of Agn Aggregates in Aqueous-Solution - Nonmetallic Oligomeric Clusters and Metallic Particles. Faraday Disc. 1991:31–44.
4. Haruta M. Catalysis: Gold Rush. Nature. 2005; 437:1098–1099. [PubMed: 16237427]
5. Aikens CM, Li S, Schatz GC. From Discrete Electronic States to Plasmons: Tddft Optical Absorption Properties of Agn (N = 10, 20, 35, 56, 84, 120) Tetrahedral Clusters. J Phys Chem C. 2008; 112:11272–11279.
6. Negishi Y, Chaki NK, Shichibu Y, Whetten RL, Tsukuda T. Origin of Magic Stability of Thiolated Gold Clusters: A Case Study on Au25(Sc6h13)18. J Amer Chem Soc. 2007; 129:11322–11323. [PubMed: 17715923]
7. Parker JF, Fields-Zinna CA, Murray RW. The Story of a Monodisperse Gold Nanoparticle: Au25l18. Acc Chem Res. 2010; 43:1289–1296. [PubMed: 20597498]
8. Qian H, Zhu M, Wu Z, Jin R. Quantum Sized Gold Nanoclusters with Atomic Precision. Acc Chem Res. 2012; 45:1470–1479. [PubMed: 22720781]
9. de Heer WA. The Physics of Simple Metal Clusters: Experimental Aspects and Simple Models. Rev Mod Phys. 1993; 65:611– 676.

10. Harb M, Rabilloud F, Simon D, Rydlo A, Lecoultre S, Conus F, Rodrigues V, Felix C. Optical Absorption of Small Silver Clusters: Ag[Sub N], (N = 4--22). J Chem Phys. 2008; 129:194108. [PubMed: 19026046]
11. Tiggesbäumker J, Köller L, Meiwes-Broer KH, Liebsch A. Blue Shift of the Mie Plasma Frequency in Ag Clusters and Particles. Phys Rev A. 1993; 48:R1749–R1752. [PubMed: 9909898]
12. Castleman AW, Khanna SN. Clusters, Superatoms, and Building Blocks of New Materials. J Phys Chem C. 2009; 113:2664–2675.
13. Zheng J, Nicovich PR, Dickson RM. Highly Fluorescent Noble-Metal Quantum Dots. Ann Rev Phys Chem. 2007; 58:409. [PubMed: 17105412]
14. Clemenger K. Ellipsoidal Shell Structure in Free-Electron Metal-Clusters. Phys Rev B. 1985; 32:1359–1362.
15. Bigioni TP, Whetten RL, Dag O. Near-Infrared Luminescence from Small Gold Nanocrystals. J Phys Chem B. 2000; 104:6983–6986.
16. Zheng J, Zhang C, Dickson RM. Highly Fluorescent, Water-Soluble, Size-Tunable Gold Quantum Dots. Phys Rev Lett. 2004; 93:art. no. 077402.
17. Peyser LA, Vinson AE, Bartko AP, Dickson RM. Photoactivated Fluorescence from Individual Silver Nanoclusters. Science. 2001; 291:103–106. [PubMed: 11141556]
18. Peyser LA, Lee TH, Dickson RM. Mechanism of Ag-N Nanocluster Photoproduction from Silver Oxide Films. J Phys Chem B. 2002; 106:7725–7728.
19. Zheng J, Dickson RM. Individual Water-Soluble Dendrimer-Encapsulated Silver Nanodot Fluorescence. J Amer Chem Soc. 2002; 124:13982–13983. [PubMed: 12440882]
20. Yu J, Patel SA, Dickson RM. In Vitro and Intracellular Production of Peptide-Encapsulated Fluorescent Silver Nanoclusters. Angew Chem Int Ed. 2007; 46:2028–2030.
21. Petty JT, Zheng J, Hud NV, Dickson RM. DNA-Templated Ag Nanocluster Formation. J Amer Chem Soc. 2004; 126:5207–5212. [PubMed: 15099104]
22. Daune M, Kekker CA, Schachman HK. Complexes of Silver Ion with Natural and Synthetic Polynucleotides. Biopolymers. 1966; 4:51–76.
23. Jensen RH, Davidson N. Spectrophotometric, Potentiometric, and Density Gradient Ultracentrifugation Studies of the Binding of Silver Ion by DNA. Biopolymers. 1966; 4:17–32.
24. Patel SA, Richards CI, Hsiang JC, Dickson RM. Water-Soluble Ag Nanoclusters Exhibit Strong Two-Photon-Induced Fluorescence. J Amer Chem Soc. 2008; 130:11602–11603. [PubMed: 18686957]
25. Driehorst T, O'Neill P, Goodwin PM, Pennathur S, Fygenson DK. Distinct Conformations of DNA-Stabilized Fluorescent Silver Nanoclusters Revealed by Electrophoretic Mobility and Diffusivity Measurements. Langmuir. 2011; 27:8923–8933. [PubMed: 21682258]
26. Ritchie CM, Johnsen KR, Kiser JR, Antoku Y, Dickson RM, Petty JT. Ag Nanocluster Formation Using a Cytosine Oligonucleotide Template. J Phys Chem C. 2007; 111:175–181.
27. Sengupta B, Ritchie CM, Buckman JG, Johnsen KR, Goodwin PM, Petty JT. Base-Directed Formation of Fluorescent Silver Clusters. J Phys Chem C. 2008; 112:18776– 18782.
28. Neidig ML, Sharma J, Yeh HC, Martinez JS, Conradson SD, Shreve AP. Ag K-Edge Exafs Analysis of DNA-Templated Fluorescent Silver Nanoclusters: Insight into the Structural Origins of Emission Tuning by DNA Sequence Variations. J Amer Chem Soc. 2011; 133:11837–11839. [PubMed: 21770404]
29. Soto-Verdugo V, Metiu H, Gwinn E. The Properties of Small Ag Clusters Bound to DNA Bases. J Chem Phys. 2010; 132:195102. [PubMed: 20499990]
30. Yu JH, Choi S, Dickson RM. Shuttle-Based Fluorogenic Silver-Cluster Biolabels. Angew Chem Int Ed. 2009; 48:318–320.
31. Richards CI, Choi S, Hsiang JC, Antoku Y, Vosch T, Bongiorno A, Tzeng YL, Dickson RM. Oligonucleotide-Stabilized Ag Nanocluster Fluorophores. J Amer Chem Soc. 2008; 130:5038–5039. [PubMed: 18345630]
32. Sharma J, Yeh HC, Yoo H, Werner JH, Martinez JS. A Complementary Palette of Fluorescent Silver Nanoclusters. Chem Comm. 2010; 46:3280–3282. [PubMed: 20442886]

33. Petty JT, Story SP, Juarez S, Votto SS, Herbst AG, Degtyareva NN, Sengupta B. Optical Sensing by Transforming Chromophoric Silver Clusters in DNA Nanoreactors. Anal Chem. 2012; 84:356–364. [PubMed: 22098274]
34. O'Neill PR, Velazquez LR, Dunn DG, Gwinn EG, Fygenson DK. Hairpins with Poly-C Loops Stabilize Four Types of Fluorescent Agn:DNA. J Phys Chem C. 2009; 113:4229–4233.
35. Petty JT, Fan C, Story SP, Sengupta B, Sartin M, Hsiang JC, Perry JW, Dickson RM. Optically Enhanced, near-Ir, Silver Cluster Emission Altered by Single Base Changes in the DNA Template. J Phys Chem B. 2011; 115:7996–8003. [PubMed: 21568292]
36. Petty JT, Fan C, Story SP, Sengupta B, St John Iyer A, Prudowsky Z, Dickson RM. DNA Encapsulation of 10 Silver Atoms Producing a Bright, Modulatable, near- Infrared-Emitting Cluster. J Phys Chem Lett. 2010; 1:2524–2529. [PubMed: 21116486]
37. Guo J, Kumar S, Bolan M, Desireddy A, Bigioni TP, Griffith WP. Mass Spectrometric Identification of Silver Nanoparticles: The Case of Ag32(Sg)19. Anal Chem. 2012; 84:5304–5308. [PubMed: 22594913]
38. Schultz D, Gwinn EG. Silver Atom and Strand Numbers in Fluorescent and Dark Ag:Dnas. Chem Comm. 2012; 48:5748–5750. [PubMed: 22552272]
39. Choi S, Yu J, Patel SA, Tzeng YL, Dickson RM. Tailoring Silver Nanodots for Intracellular Staining. Photochem Photobiol Sci. 2011; 10:109–115. [PubMed: 21063587]
40. Lavis LD, Raines RT. Bright Ideas for Chemical Biology. ACS Chem Biol. 2008; 3:142–155. [PubMed: 18355003]
41. Larson DR, Zipfel WR, Williams RM, Clark SW, Bruchez MP, Wise FW, Webb WW. Water-Soluble Quantum Dots for Multiphoton Fluorescence Imaging in Vivo. Science. 2003; 300:1434–1436. [PubMed: 12775841]
42. Betzig E, Patterson GH, Sougrat R, Lindwasser OW, Olenych S, Bonifacino JS, Davidson MW, Lippincott-Schwartz J, Hess HF. Imaging Intracellular Fluorescent Proteins at Nanometer Resolution. Science. 2006; 313:1642–1645. [PubMed: 16902090]
43. Rust MJ, Bates M, Zhuang XW. Sub-Diffraction-Limit Imaging by Stochastic Optical Reconstruction Microscopy (Storm). Nature Meth. 2006; 3:793–795.
44. Hess ST, Girirajan TPK, Mason MD. Ultra-High Resolution Imaging by Fluorescence Photoactivation Localization Microscopy. Biophys J. 2006; 91:4258–4272. [PubMed: 16980368]
45. Jablonski A, Hsiang J, Bagchi P, Hull N, Richards CI, Fahrni CJ, Dickson RM. Signal Discrimination between Fluorescent Proteins in Live Cells by Long-Wavelength Optical Modulation. J Phys Chem Lett. 2012; 3:3585–3591. [PubMed: 23419973]
46. Fan C, Hsiang JC, Jablonski AE, Dickson RM. All-Optical Fluorescence Image Recovery Using Modulated Stimulated Emission Depletion. Chem Sci. 2011; 2:1080–1085. [PubMed: 22262992]
47. Dertinger T, Heilemann M, Vogel R, Sauer M, Weiss S. Superresolution Optical Fluctuation Imaging with Organic Dyes. Angew Chem Int Ed. 2010; 49:9441–9443.
48. Patel SA, Cozzuol M, Hales JM, Richards CI, Sartin M, Hsiang JC, Vosch T, Perry JW, Dickson RM. Electron Transfer-Induced Blinking in Ag Nanodot Fluorescence. J Phys Chem C. 2009; 113:20264–20270.
49. Richards CI, Hsiang JC, Senapati D, Patel S, Yu J, Vosch T, Dickson RM. Optically Modulated Fluorophores for Selective Fluorescence Signal Recovery. J Amer Chem Soc. 2009; 131:4619–4621. [PubMed: 19284790]
50. Richards CI, Hsiang JC, Dickson RM. Synchronously Amplified Fluorescence Image Recovery (Safire). J Phys Chem B. 2010; 114:660–665. [PubMed: 19902923]
51. SantaLucia J Jr, Hicks D. The Thermodynamics of DNA Structural Motifs. Ann Rev Biophys Biomol Struct. 2004; 33:415–440. [PubMed: 15139820]
52. Shah P, Rorvig-Lund A, Ben Chaabane S, Thulstrup PW, Kjaergaard HG, Fron E, Hofkens J, Yang SW, Vosch T. Design Aspects of Bright Red Emissive Silver Nanoclusters/DNA Probes for Microrna Detection. Acs Nano. 2012; 6:8803–8814. [PubMed: 22947065]
53. Guo W, Yuan J, Dong Q, Wang E. Highly Sequence-Dependent Formation of Fluorescent Silver Nanoclusters in Hybridized DNA Duplexes for Single Nucleotide Mutation Identification. J Amer Chem Soc. 2010; 132:932–934. [PubMed: 20038102]

54. Sengupta B, Springer K, Buckman JG, Story SP, Abe OH, Hasan ZW, Prudowsky ZD, Rudisill SE, Degtyareva NN, Petty JT. DNA Templates for Fluorescent Silver Clusters and I-Motif Folding. J Phys Chem C. 2009; 113:19518–19524.

55. Li J, Zhong X, Cheng F, Zhang JR, Jiang LP, Zhu JJ. One-Pot Synthesis of Aptamer-Functionalized Silver Nanoclusters for Cell-Type-Specific Imaging. Anal Chem. 2012; 84:4140–4146. [PubMed: 22482827]

56. Yeh HC, Sharma J, Shih IM, Vu DM, Martinez JS, Werner JH. A Fluorescence Light-up Ag Nanocluster Probe That Discriminates Single-Nucleotide Variants by Emission Color. J Amer Chem Soc. 2012; 134:11550–11558. [PubMed: 22775452]

Biographies

Jeff Petty joined Furman University in 1995. His interest in chemistry developed at Furman with Tony Arrington and Lon Knight, Jr., the University of California, Berkeley with C. Bradley Moore, and Los Alamos National Laboratory with Richard Keller. He has mentored 50 undergraduates in biophysical chemistry research. His webpage is: http://chemistry.furman.edu/profile.php?shortname=petty

Sandra Story received microbiology degrees from the University of Massachusetts, Amherst, University of Nevada, Las Vegas, and Clemson University. She is interested in environmental microbiology. Under the direction of Dr. Melissa Riley at Clemson University, she learned separation methods that have been used for the characterization of DNA-bound silver clusters.

Jung-Cheng Hsiang is a PhD student in the Georgia Institute of Technology's School of Physics. He joined Robert Dickson's laboratory in 2006. Since then, he has studied the mechanism and applications of both silver cluster emitters and the optical modulation of these and other compounds.

Robert Dickson earned degrees from Haverford College and The University of Chicago. He joined Georgia Tech's faculty in 1998 where he has pioneered the development and use of silver cluster and modulatable organic fluorophores to selectively recover weak signals buried within high-background biological environments. His webpage is: http://www.chemistry.gatech.edu/faculty/Dickson/

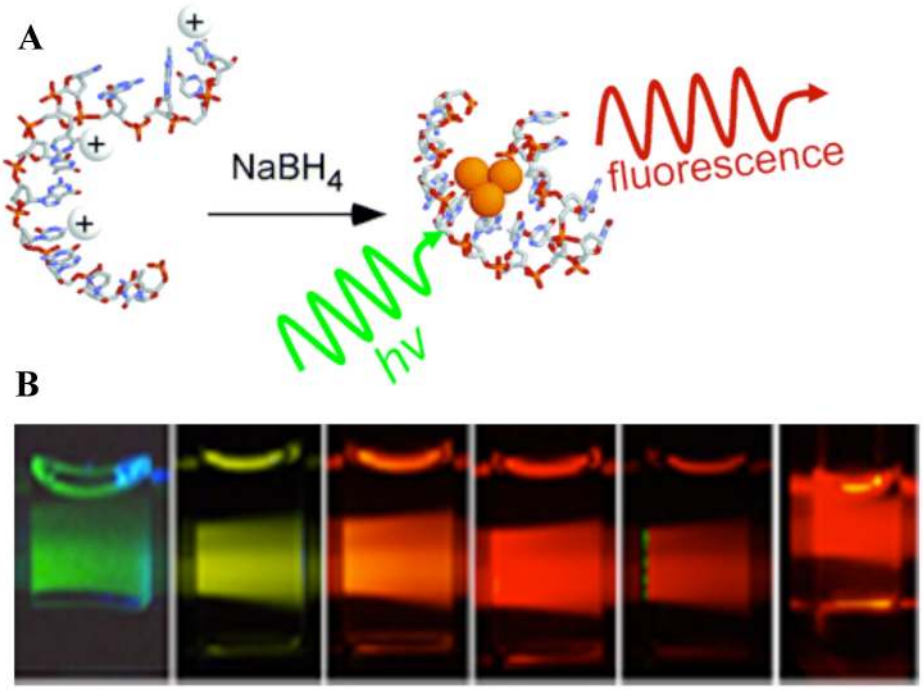

Figure 1.

A. (Reproduced from Ref. 21) Schematic of DNA-conjugated silver cluster creation. Ag^+ (white ion) preferentially associates with the nucleobases in single DNA strands. Subsequent reduction with BH_4^- produces small emissive agglomerates of neutral Ag atoms (orange spheres). B. Examples of some of the wide range of spectrally pure Ag cluster emitters that can be made changing buffer conditions and DNA sequences (From Ref. 39 - Reproduced by permission of The Royal Society of Chemistry (RSC) on behalf of the European Society for Photobiology, the European Photochemistry Association, and RSC). Emission maxima (sequence) from left to right: 523 nm (C_{20}), 562 nm ($AATTC_{12}$), 590 nm ($CGAAC_{12}$), 615 nm ($CGCGC_{12}$), 635 nm ($ATATC_8$), 670 nm ($GGGGC_8$). Both the primary sequence and reaction conditions determine the final clusters formed and their associated photophysics.

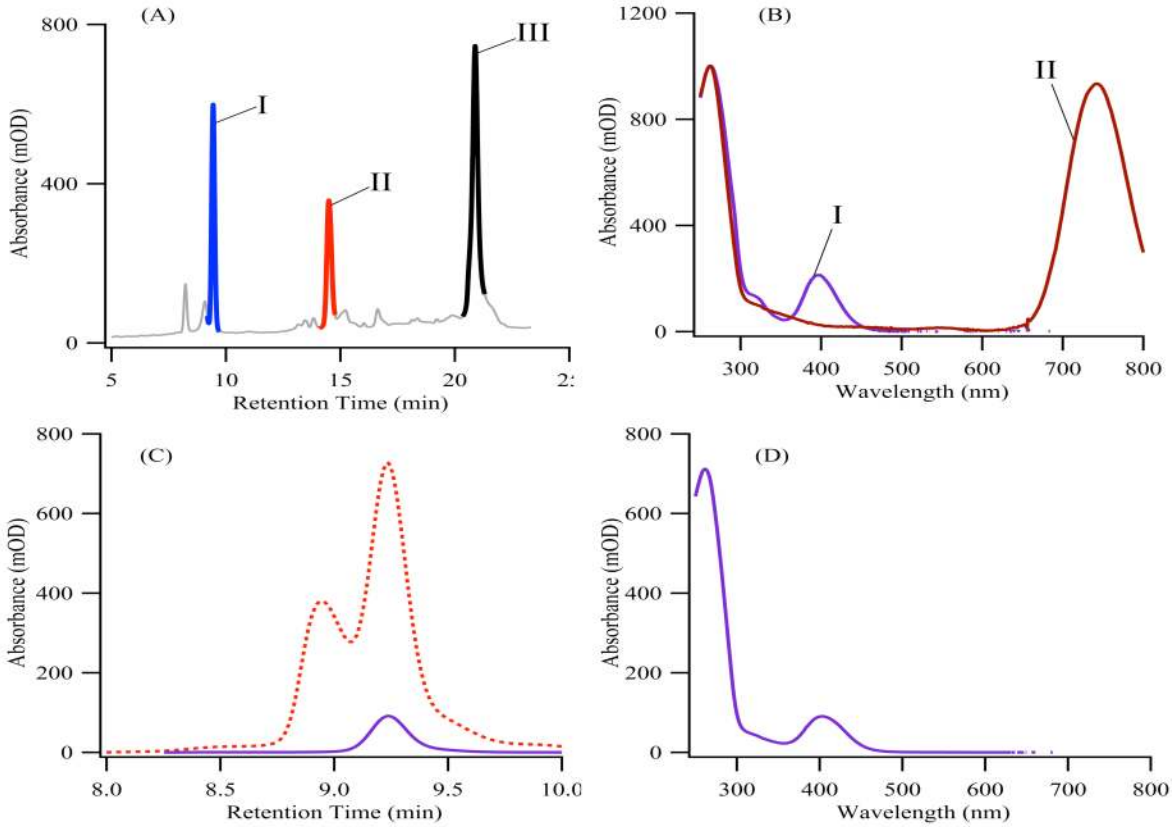

Figure 2.

(Adapted from Ref. 33) Chromatographic purification of silver cluster-DNA conjugates. (A) The reversed-phase chromatogram at 260nm absorbance shows all species containing the $C_3AC_3AC_3TC_3A$ ss-DNA scaffold. (B) The absorption spectra corresponding to peaks I and II from (A) show the distinct spectra associated with each resolved cluster.[36] (C) A size exclusion chromatogram for a violet-absorbing cluster bound to a DNA strand was acquired at 260 nm (red dotted line) and at 400 nm (solid violet line). Correspondence between the DNA- and cluster-specific chromatograms identifies the conjugate, whose spectrum is provided in (D).[33]

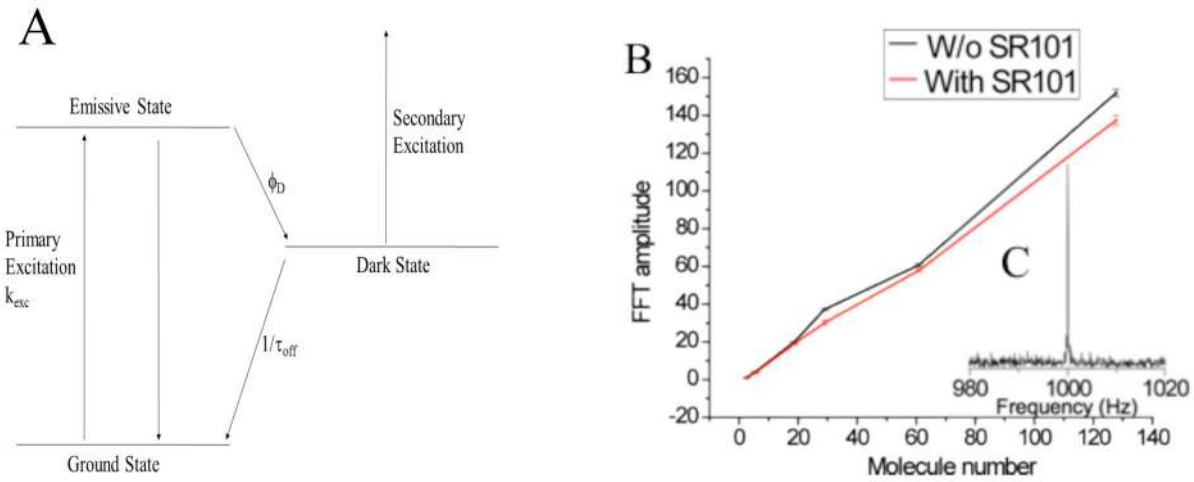

Figure 3.

(A) Schematic energy level model of cluster-DNA conjugate photophysics. Fluorescence is derived from primary laser-induced cycling through the ground and emissive states. Inverse transition rates into and out of the dark state define $\tau_{on} = (k_{exc}\ \Phi_D)^{-1}$ and $\tau_{off} = k_{off}^{-1}$ respectively. Decay from the dark state occurs by both natural decay and secondary laser-induced optical excitation, and the latter provides a faster and controllable channel for repopulating the emissive manifold of state. Right panel: Ag cluster emission is readily recovered from overwhelming non-modulatable sulforhodamine 101 (SR101) background. Fluorescent background from SR101 is ~15,000 counts/second. Dilution of Ag cluster emitters decreases total fluorescence, but unlike FCS, the Fourier transform amplitude is linear with the number of modulatable emitters (B), allowing separation and recovery of the cluster signal (peak at 1kHz, C) from SR101 emission at 0 Hz.

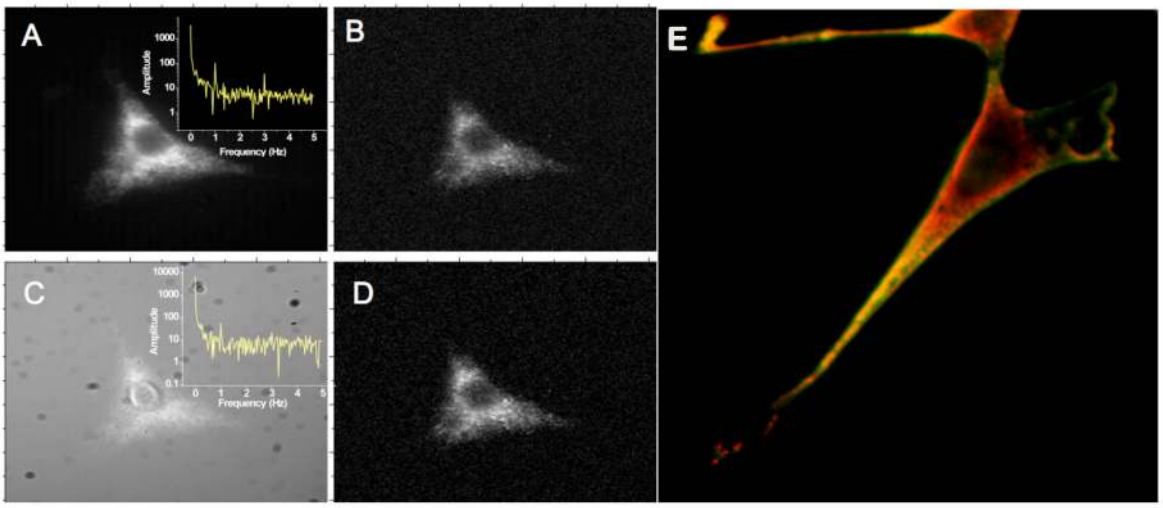

Figure 4.

Silver clusters targeted to the surface of fixed cells. (A–D, entire image width: 68μm, reproduced from Ref. 49) 710-nm cluster emitters were conjugated to anti-heparin and bound to fixed NIH-3T3 cells. The entire field of view is modulated at 1Hz with synchronous CCD detection, yielding only 1% modulation depth due to the very low intensity secondary illumination used. The 1-Hz modulation peak is readily observed (A, inset) and enables demodulation through plotting Fourier amplitude at 1 Hz for each pixel to yield B. Addition of Cy5 obscures the same cell in panel C, but the 1-Hz modulation peak is still observed. Demodulation removes this heterogeneous Cy5 background to recover the original cell image in D. (E) Multiple clusters can be used to label fixed cells simultaneously. Red and green-emitting clusters are targeted to mitochondria and heparin sulfate (cell surface) within the same fixed cell by coupling different DNA sequences to the different antibodies.[39]

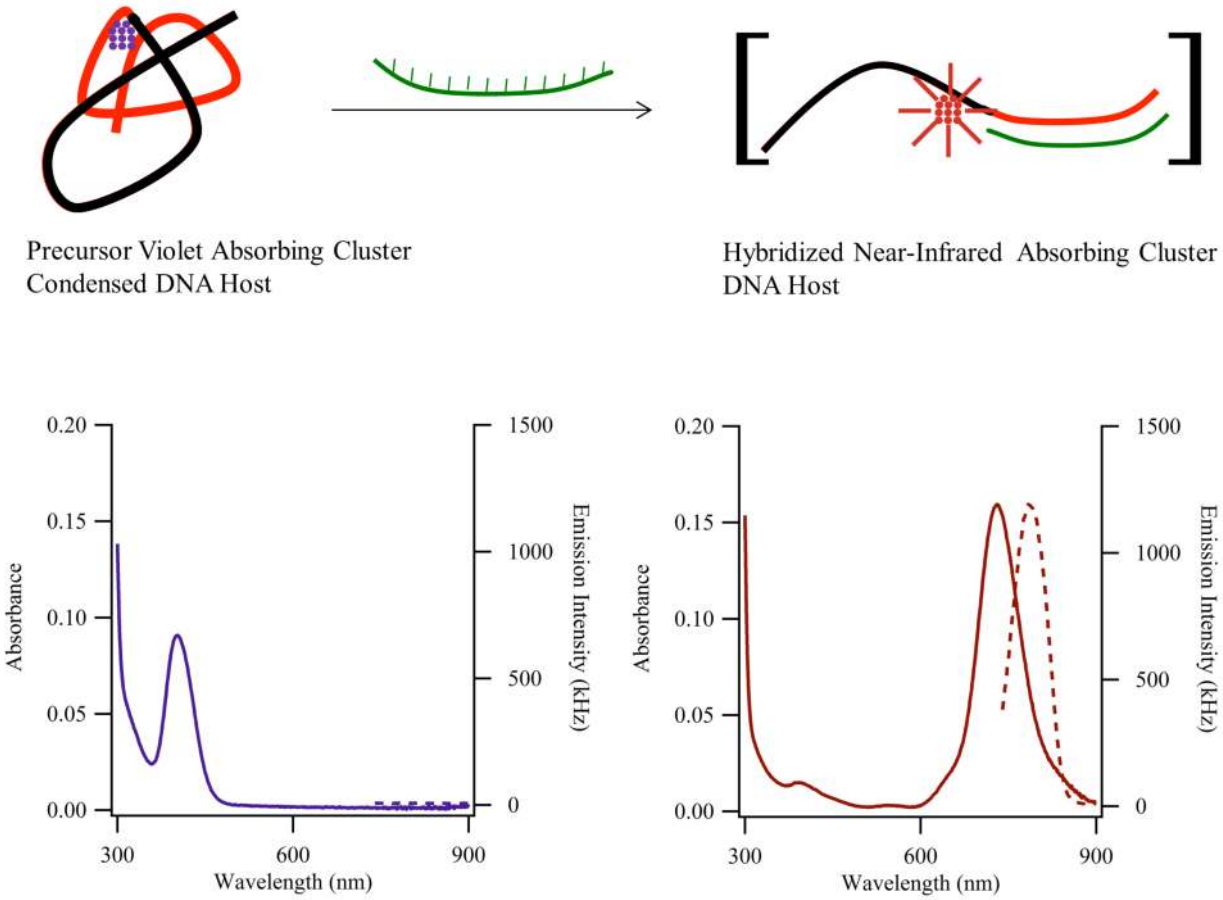

Figure 5.

(Adapted from Ref. 33) The reaction summarizes how the structure of the sensor strand and the stoichiometry of the cluster are linked with the changes in the absorption (solid lines – left axes) and emission (dotted lines – right axes) spectra in the lower panels. (Left) The sensor is comprised of a cluster template (black portion) and a recognition site (red portion) and is folded by an ~11 silver atom cluster (violet) with τ_{max} = 400 nm and minimal near-infrared emission. (Right) Addition of the complementary strand (green) opens the sensor strand, and the absorption of the resulting ~11 atom cluster red-shifts to 730 nm, and the associated emission is magnified.

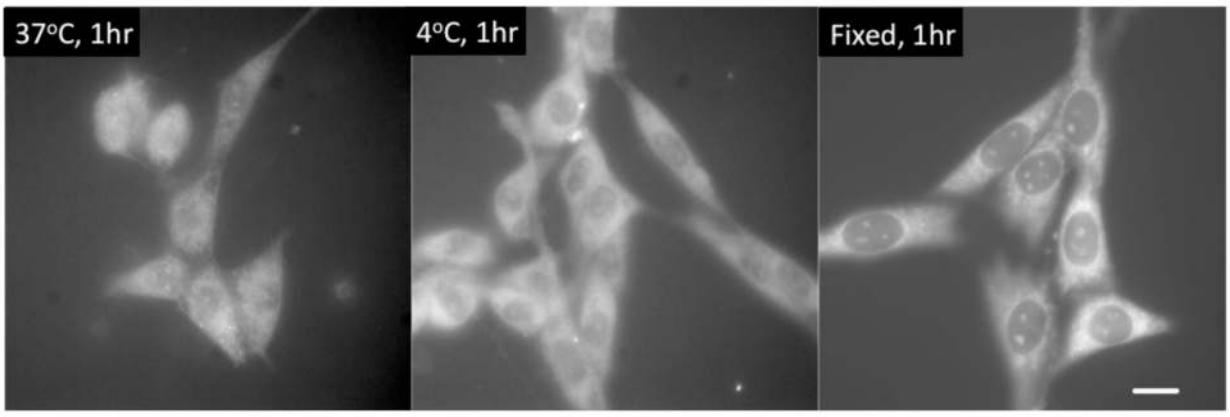

Figure 6.
Live (left and center) and (right) fixed cells labeled with peptide-encapsulated silver clusters. Emission is quite bright even though peptide-cluster quantum yields are only ~3%. Unlike most DNA-encapsulated clusters, peptide-silver cluster emission is quite stable in live cells at 37°C. Scale bar: 30μm. (Reproduced from Ref. 20, with labels added)

Table 1

Silver Atom Stoichiometries with Different Templates

Sequence (excitation and emission maxima)	Ag:Oligonucleotide
CCC CAA CTC C (λ_{ex} = 540 nm/λ_{em} = 630 nm)	4.8 ± 0.4
CCCTAACTCCCC (λ_{ex} = 650 nm/λ_{em} = 710 nm)	5.9 ± 0.5
$C_3AC_3AC_3TC_3A$ (λ_{ex} = 750 nm/λ_{em} = 810 nm)	9.6 ± 0.8
$C_3AC_3AC_3GC_3A$ (λ_{ex} = 720 nm/λ_{em} = 770 nm)	10.0 ± 1.7
$C_3AC_3AC_3AC_3G$ (λ_{ex} = 820 nm/λ_{em} = 900 nm)	9.1 ± 0.7
$C_3AC_3AC_3TC_3A$ TT CCCGCCGCTGGA (λ_{max} = 400 nm)	11.1 ± 1.1
$C_3AC_3AC_3TC_3A$ TT CCCGCCGCTGGA GGGCGGCGACCT (λ_{ex} = 730 nm/λ_{ex} = 785 nm)	11.5 ± 1.2